Jestr

Journal of Engineering Science and Technology Review 15 (5) (2022) 189 - 203

Research Article

JOURNAL OF
**Engineering Science and Technology Review**

www.jestr.org

# Bending Analysis of 2-D Functionally Graded Porous Beams Based on Novel High Order Theory

**G. Chandra Mohana Reddy* and Nathi Venu Kumar**

*Department of Mechanical Engineering, School of Technology, GITAM, Hyderabad, India.*

Received 17 February 2022; Accepted 24 August 2022

***Abstract***

For modern structures and components, advanced engineering materials are preferred whose properties change continuously in more than one direction. In particular, the 2-D Functionally Graded Materials (2-D FGMs) have shown added effective properties, which will lead to avoid delamination and stress concentration. To research bending response of Functionally Graded Beams (FGBs), a novel shear strain shape function is chosen and considering the even and uneven porosity distributions. Material properties of even and uneven porosity distributions along the length and thickness directions of FGBs are varied in two directions by power-law. Present theory includes the influence of thickness stretching. This theory also fulfills the nullity of shear stresses in transverse direction on upper and lower side of the beam, thus avoiding use of a correction factor to accurately estimate shear stresses. The principle of virtual displacements is employed to develop equilibrium equations for porous FGBs. Navier's method is used to obtain solutions to porous FGBs for Simply Supported (SS) boundary conditions. To ascertain accuracy, the developed theory is justified with numerical results of perfect and porous FGBs available in the open source. Influence of exponents, porosity volume fraction, thickness ratios, and aspect ratios on dimensionless deflections and stresses are studied. It can be observed that the effect of porosity coefficient on bending behavior of FG beams subjected to uniform transverse load, transverse deflection increases as the porosity coefficient increases and this effect is more prominent with high values of porosities from 20% to 30%. So the porosity parameter is a crucial parameter that must be considered in design of modern structures and the percentage of porosity in structure can be effected considerably in its performance and response.

*Keywords:* 2-D FGBs; 5$^{th}$ order theory; Navier's method; Porosity beams.

## 1. Introduction

Japanese scientists have introduced this Functionally Graded Materials (FGM) in the year 1984. These materials are considered as a special class in composite materials because of their superior properties like light weight, wear resistance, prolonged fatigue life, high strength and stiffness, and exceptional thermal insulation, which change from one surface to another. In the present scenario, these materials are used in many engineering applications like space structures, spacecraft, and nuclear reactors. As per power – law, the volume fraction and material composition are changed along with its length and thickness directions. Due to these features, functionally graded materials avoid delaminating failure, material discontinuity, deflections, and diminishing stress levels.

By Timoshenko beam theory, analyzed bending characteristic of two dimensional FG beam. According to this theory, mechanical properties of beam were varied both directions [1]. Presented the subject of FG beam under sinusoidal loads for investigation of free vibration and bending characteristics by using HSDT. Consider various patterns of porosity distributions to this investigation [2].Using various theories of two- dimensional and quisi three-dimensional, to analyzed characteristics of FG beams with simply supported (SS) under various conditions like static bending, elastic buckling, and free vibration [3]. Under UDL to the developed exact analytical results of simply supported (SS) beam. Specific analytical formulas were expressed by using 3$^{rd}$ order shear deformation and compared to the existing numerical results and classical analytical ones [4]. Presented behavior of bending of FG composite curved beam based on theory of higher-order with normal deformation. This investigation considers effect of shear and normal transverse deformations [5].

Presented characteristics of static, free vibration, and elastic buckling of micro plates with FG porous material by a general 3$^{rd}$ order plate theory. From Navier's equations, the analytical solutions were obtained [6]. To propose new porosity distribution to determining the static behavior of sandwich FG plates. Across plate thickness, the material properties of functionally graded material layers were varied continuously as per sigmoid function or power-law in terms of volume fractures of the constituents [7]. Developed governing equations to auxiliary functions and used them to calculate vibration and static behavior of FG beams with varying material properties continuously [8].Bending analysis of FG curved beam was presented by using higher-order theory with shear deformation effect and thickness stretching. Sandwich beams with FG in various symmetric and non-symmetric core or skins under the UDL were considered [9].To investigated elastic Buckling, and static response of FG saturated beam with porous resting on Winkler elastic base. Using theory of shear deformation with higher-order, the beam was made with Biot constitutive law [10].

*E-mail address: cnreddy@gmail.com
ISSN: 1791-2377 
doi:10.25103/jestr.155.24

Free vibration and static responses were investigated of advanced composite material plates by using the theory of refined simple 1st order shear deformation. Distribution of shear stress and the shear strain was in a parabolic shape [11]. From shear deformation theory with higher-order to represent bending characteristics of FG porous rectangular pates. Due to effect of normal deformation and shear strain this theory does not require any shear correction factor [12]. FG porous beams are subjected to calculate bending characteristics with effects of temperature and moisture. Consider the normal strain and shear strain effects of this investigation [13]. Free vibration, Buckling, and static responses of HSD were investigated for higher-order beams with FG material. According to the distribution of Power-law, the properties of FG material beams were varied through-thickness [14].By using classical and plate theory of shear deformation with the first order, investigate static, free vibration, and elastic buckling responses of FG porous micro-plates. To obtain analytical results of SS rectangular plates by utilizing Navier technique [15].

Investigated free vibration behavior of bi-directional FGPs by refined shear deformation theory with first order. From Lagrange equations, equations of motion were developed [16]. Based on HSDT to developed bending results of FG porous plates with rectangular shape. To verify boundary conditions with no constraints on top and bottom surfaces of plate [17]. Theory of higher-order was presented for static behavior of pates with FG material. By using principle of effective work to derived governing equations, various boundary conditions, and force and moment resultants of HSDTs [18]. To investigate bending results of FG ceramic-metal porous plates by using the theory of shear deformation with higher order. It's required no shear correction factor due to the effect of normal deformation and shear strain [19]. With theory of refined hyperbolic shear deformation to developed analytical solutions for free vibration results of FG beams in which stretching effect was included. Based on power-law distribution, the modulus of elasticity of beam varied in volume fractions of constituents [20].

Theory of unified shear deformation was developed based on displacement for analysis of advanced composite plates and beams. This theory considered shape function in terms of transverse shear deformation effect [21]. Sandwich FB beam with various symmetric and non-symmetric was subjected to static behavior to this investigation considered thickness stretching effects and shear deformation [22].Developed characteristics of bending and elastic buckling of beam with FG material from the theory of 5Th order shear and normal deformation. At top and bottom surfaces of beam boundary conditions were satisfied with no shear correction factor [23]. Symmetric and anti-symmetric functions were developed and compare classical power distribution. Symmetric Power-law distributions were proposed and sigmoid functions were anti-symmetric. Micromechanical properties of FG material were homogenized and derived the effective material properties on basis of the Voigt model [24].Transverse stresses are satisfied at bottom and top of FG plates with HSDT with 8 unknown based on 12 unknown of HSDT [25].

With the beam theory of Timoshenko presented buckling and static analysis of FG porous beam. Porous composite material properties such as elasticity module and mass density were distributed in different patterns in the thickness direction [26]. Analyzed boundary conditions to solve the problem of electrostatic FG Kirchhoff free plate under transverse load distribution per area and bending load per length [27]. Static analysis was investigated of FG nano-plates by the theory of sinusoidal shear deformation. It satisfies the distribution of free transverse shear stress and sinusoidal transverse shear stress on top and bottom surfaces of plate with no using of shear correction factor [28]. Presented RSDT, for analysis of static and free vibration of FG beams. The theory of shear deformation did not need a shear correction factor. To derived motion equations from Hamilton's principle [29]. For analysis of bending of FG plates to developed analytical solutions and formulation without enforcing zero transverse shear stress on surface of the plate by using HSDT [30].

Two directional FG beams behavior of free vibration was presented with various boundary conditions. Properties of beam material were changed by accommodating various gradation exponents in x and z directions [31].FG material plates were analyzed to determined behavior of vibration and static based on theory of HSD with modification of transverse displacement by finite element model [32].FG beams were analyzed to determining static bending and vibration analysis with various theories of HSD. With transverse shear strain boundary settings to satisfy top and bottom surface of beam [33].1storder beam theory with shear deformation was developed to determining static and vibration of FG beams. Transverse shear stiffness improved was by using plane stress and aquarium equation [34]. Developed 1st order theory with shear deformation for bending characteristics of FG plates. On 1st order plate theory with shear deformation governing equations of axial and transverse deformations of FG plates are derived [35].On classical,1st order plate theory with shear deformation, investigated static behavior, vibration, and buckling responses of FG porous micro-plates [36].

## 2. Material Selections:

Consider a rectangular beam of FGM to this research work, and made up of metal and ceramic with length L, breadth b, and thickness h in x, y, and z directions shown in Figure 1. To be assumed Properties of beam material are varying continuously along x and z- directions. Here, the upper face($z = +h/2$)is with metal and lower face ($z = -h/2$)is with ceramic. Middle surface of beam is reference surface i.e. (z=0).

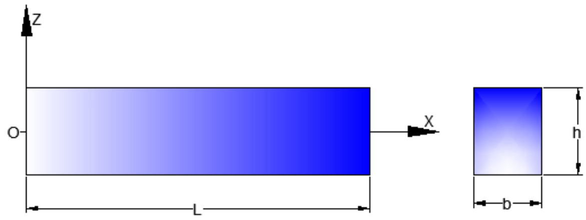


**Fig. 1** The geometry of FG porous beam

The FG porous beam's properties continuously vary due to changes in volume fraction of constituent materials. Functional relationship among thickness coordinate and property of the material are to be assumed. Volume fraction of metal ($V_m$) as per to power-law in two directions(x, z) can be expressed as:

$$V_f(x,z) = \left(\frac{z}{h}+\frac{1}{2}\right)^{pz}\left(\frac{x}{L}+\frac{1}{2}\right)^{px} \quad (1)$$

Where h and z represent the thickness of beam and thickness coordinate respectively. The origin (O) of rectangular beam's mid surface (x, y) as $z \in [-h/2, h/2]$. Figure 2 shows the relation between volume fraction evolution, length, and thickness of beams through power-law exponent values. Here p indicates the volume fraction behavior along beam's thickness and length.

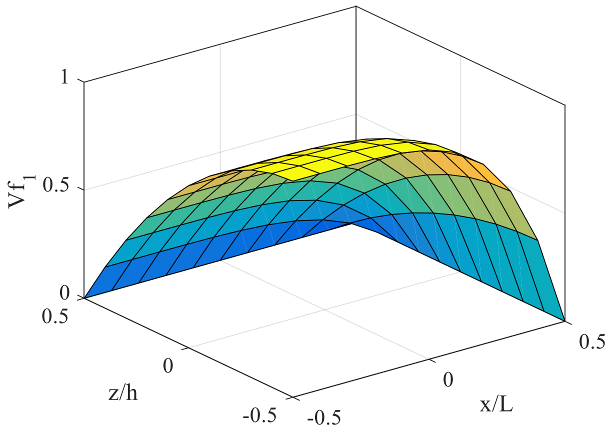


**Fig. 2** Changes of volume fraction $V_f$ across thickness and length of FG beam with different values of gradation exponents.

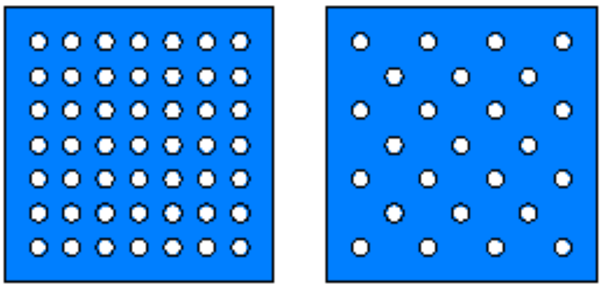

**Fig. 3** Two directional FGB with even and uneven porosity

## 2.1. Formulation for Functionally Graded Porous Beams:

Porosities appeared as a defect in functionally graded beam because of technical and penetration problems in production process. Porosities in beam are two types namely, even and uneven as shown in Figure 3. Modulus elasticity (E), mass density (ρ), and Poisson's ratio (μ) are material properties of beam and are determined from modified formula in which α represents porosity volume fraction.

Material properties of FG porous beam (even distribution) can be defined as:

$$P(x,z) = (P_c - P_m)\left(\frac{z}{h}+\frac{1}{2}\right)^{pz}\left(\frac{x}{L}+\frac{1}{2}\right)^{px} + P_m - \frac{\alpha}{2}(P_m + P_c) \quad (2)$$

Here α represents the porosity coefficient and defined as ratio between void volume and complete volume ($0 \le \alpha < 1$). The subscripts m denote metal and c denote ceramic phases '$P_x$' and '$P_z$' are non-negative variables that define AFG (along the axis) and FG (along with thickness) power indexes, respectively, which are related to volume fraction change along axis and thickness.

Material properties of beam, modulus of elasticity 'E', Poisson's ratio '$v$' and density 'ρ' of FGM porous beam (even) is given below:

$$E(x,z) = (E_c - E_m)\left(\frac{z}{h}+\frac{1}{2}\right)^{pz}\left(\frac{x}{L}+\frac{1}{2}\right)^{px} + E_m - \frac{\alpha}{2} \quad (3)$$

$$\rho(x,z) = (\rho_c - \rho_m)\left(\frac{z}{h}+\frac{1}{2}\right)^{pz}\left(\frac{x}{L}+\frac{1}{2}\right)^{px} + \rho_m - \frac{\alpha}{2}(\rho_m + \rho_c) \quad (4)$$

Material properties of beam, modulus elasticity 'E' and density 'ρ' of FGM porous beam (uneven) is given below

$$E(x,z) = (E_c - E_m)\left(\frac{z}{h}+\frac{1}{2}\right)^{pz}\left(\frac{x}{L}+\frac{1}{2}\right)^{px} + E_m - \frac{\alpha}{2}(E_m + E_c)\left(1 - \frac{2|z|}{h}\right) \quad (5)$$

$$\rho(x,z) = (\rho_c - \rho_m)\left(\frac{z}{h}+\frac{1}{2}\right)^{pz}\left(\frac{x}{L}+\frac{1}{2}\right)^{px} + \rho_m - \frac{\alpha}{2}(\rho_m + \rho_c)\left(1 - \frac{2|z|}{h}\right) \quad (6)$$

## 2.2. Displacement Field and Constitutive Equations:

Consider functionally graded rectangular beam as shown in Figure.1 for variation formulation and analytical results. Static behavior of FG beams depends upon transverse shear and normal deformations. Therefore any refinements of classical beam theories are generally meaningless, so effect of transverse shear and normal strain should be considered. In this view, the present theory has important features as follows.

Shear deformation theory is considered to present the displacement equations using Reddy's higher order shear deformation theory (HSDT) with novel shear strain function.

$$U(x,z,t) = u_0(x,t) - z\frac{\partial w_0}{\partial x}(x,t) + f(z)\left(\emptyset(x,t) + \frac{\partial w_0}{\partial x}(x,t)\right) \quad (7)$$

$$W(x,z,t) = w_0(x,t) \quad (8)$$

From above equations, U is axial displacement and w transverse displacements and $u_0$, $w_0$ are axial displacement at any point on neutral axis, $\frac{\partial w_0}{\partial x}$ is bending slope and $\phi$ is shear slope. For determining the distribution of transverse shear deformation, shape function $i.e. f(z)$ is used.

$$\varepsilon_x = \frac{\partial U}{\partial x} = \frac{\partial u_0}{\partial x} - z\frac{\partial^2 w_0}{\partial x^2} + f(z)\left(\frac{\partial \phi}{\partial x} + \frac{\partial^2 w_0}{\partial x^2}\right) \quad (9)$$

$$\varepsilon_z = \frac{\partial w}{\partial z} = 0 \quad (10)$$

$$\gamma_{xz} = f'(z)\left[\emptyset + \frac{\partial w_0}{\partial x}\right] \quad (11)$$

$$f(z) = \frac{h}{\pi} * sin\left[\frac{\pi * z}{h}\right] - \frac{z}{n*\pi}\left(1 - \frac{1}{n} * \left(\frac{2}{h}\right)^{n-1} * z^{n-1}\right) \quad (12)$$

$$f'(z) = \frac{h}{\pi} * \mathrm{Sin}\left[\frac{\pi}{h}\right] - \frac{1}{n*\pi}\left(1 - \frac{1}{n} * \left(\frac{2}{h}\right)^{n-1} * (n-1)z^{n-2}\right) \quad (13)$$

Based on the Hooks law, the two directional stress strain relation is as follows,

$$\sigma_x = \frac{E(x,z)}{1-\mu^2} \quad (14)$$

$$\tau_{xz} = \frac{E(x,z)}{2(1+\mu)}\gamma_{xz} \tag{15}$$

### 2.3. Governing Differential Equations:

From principle of virtual displacements, the governing equations can be derived. The principle of virtual work in present can yield,

$$\int_0^T \delta(U+V-K)\,dt = 0 \tag{16}$$

Where,

δU is variation of strain energy, δV is variation of work done , δk is variation of kinetic energy and t is time.

From principle of virtual displacements, the governing differential equation of virtual strain energy and work done can be given as,

$$\delta U = \int_0^L \int_{-\frac{h}{2}}^{\frac{h}{2}} (\sigma_x \delta\varepsilon_x + \tau_{xz}\delta\gamma_{xz})dzdx \tag{17}$$

$$\delta V = -\int_0^L q\delta w_0\, dx \tag{18}$$

The bending stress of beam in terms of virtual strain energy and work done can be shown by:

$$B = \delta U + \delta V = 0 \tag{19}$$

$$= \int_0^L \int_{-\frac{h}{2}}^{\frac{h}{2}} (\sigma_x \delta\varepsilon_x + \tau_{xz}\delta\gamma_{xz})dzdx - \int_0^L q\delta w_0\, dx = 0 \tag{20}$$

$$= \int_0^L \int_{-h/2}^{h/2} \left(\sigma_x \delta\left(\frac{\partial u_0}{\partial x} - z\frac{\partial^2 w_0}{\partial x^2} + f(z)\left(\frac{\partial \phi}{\partial x} + \frac{\partial^2 w_0}{\partial x^2}\right)\right) + \tau_{xz\delta} f'(z)\left[\emptyset + \frac{\partial w_0}{\partial x}\right]\right) dzdx - \int_0^L q\delta w_0\, dx = 0 \tag{21}$$

$$= \int_0^L \left(\frac{\partial N_x \delta u_0}{\partial x} - \frac{\partial^2 M_b \delta w_0}{\partial x^2} + \frac{\partial M_s \delta\emptyset}{\partial x} + \frac{\partial^2 M_s \delta w_0}{\partial x^2} + Q_{xz}\delta\emptyset + \frac{\partial Q_{xz}\delta w_0}{\partial x}\right) dx - \int_0^L q\delta w_0\, dx = 0 \tag{22}$$

$$\begin{bmatrix} N_x \\ M_b \\ M_s \end{bmatrix} = \int_{-\frac{h}{2}}^{\frac{h}{2}} \sigma_x \begin{Bmatrix} 1 \\ z \\ f(z) \end{Bmatrix} dz \tag{23}$$

$$Q_{xz} = \int_{-\frac{h}{2}}^{\frac{h}{2}} \tau_{xz} f'(z) dz \tag{24}$$

Where,
$N_x$ is axial resultant force, $M_b$ is resultant bending moment, $M_s$ is resultant moment due to shear deformation and $Q_{xz}$ is resultant shear forces.

By integrating the displacement gradations, the governing equations of equilibrium can be derived.

$$\delta u_0 : \frac{\partial}{\partial x} N_x = 0 \tag{25}$$

$$\delta w_0 : \frac{\partial^2}{\partial x^2} M_b - \frac{\partial^2}{\partial x^2} M_x + q - \frac{\partial}{\partial x} Q_{xz} = 0 \tag{26}$$

$$\delta\emptyset : \frac{\partial}{\partial x} M_s + Q_{xz} = 0 \tag{27}$$

### 2.4 Equations of Motion in Terms of Displacements

Analytical results of SS boundary conditions are obtained with the help of Navier techniques. To this reason the displacement functions are expressed as a product of undetermined coefficients ($\delta u_0$ , $\delta w_0$ $and$ $\delta\emptyset$) and satisfy the governing equations at x=0 and x=L.

$$u_0(x,t) = \sum_{j=1,3,5}^{m} A_{j\theta_j}(x) e^{i\omega t}, \qquad \theta_j(x) = \left(x+\frac{L}{2}\right)^{pu}\left(x-\frac{L}{2}\right)^{qu} x^{m-1} \tag{28}$$

$$w_0(x,t) = \sum_{j=1,3,5}^{m} B_j \varphi_j(x) e^{i\omega t}, \qquad \varphi(x) = \left(x+\frac{L}{2}\right)^{pw}\left(x-\frac{L}{2}\right)^{qw} x^{m-1} \tag{29}$$

$$\emptyset(x,t) = \sum_{j=1,3,5}^{m} C_{j\psi_j}(x) e^{i\omega t}, \qquad \psi_j(x) = \left(x+\frac{L}{2}\right)^{p\phi}\left(x-\frac{L}{2}\right)^{q\phi} x^{m-1} \tag{30}$$

where $u_0$,$w_0$ and $\phi$ are unknown coefficients, α = *πm/ L* and is natural frequency of porous beam. Complex number $i=\sqrt{-1}$ is used in determining unknown coefficients $A_j$, $B_j$, and $C_j$. The transverse load q act uniformly on upper surface of beam and also extended in Fourier series

$$q = \sum_{m=1,3,5}^{\infty} \frac{4q_0}{m\pi} sin\alpha x \tag{31}$$

Where $q_0$ is maximum intensity of load at center of rectangular beam. By substituting eq.28, eq. 29 and eq. 30 into eq. 19, the analytical solution can be obtained from the following equations.

$$S_{11}(i,j) = \frac{E(x,z)}{1-\mu^2}\int_{-\frac{h}{2}}^{\frac{h}{2}} \theta_{i,x}\theta_{j,x}\, dx. \tag{32}$$

$$S_{12}(i,j) = \frac{E(x,z)}{1-\mu^2}\int_{-\frac{h}{2}}^{\frac{h}{2}} \theta_{i,x}\varphi_{j,xx}\, dx \tag{33}$$

$$S_{13}(i,j) = \frac{E(x,z)}{1-\mu^2}\int_{-\frac{h}{2}}^{\frac{h}{2}} \theta_{i,x}\psi_{j,x}\, dx \tag{34}$$

$$S_{22}(i,j) = \frac{E(x,z)}{1-\mu^2}\int_{-\frac{h}{2}}^{\frac{h}{2}} \varphi_{i,xx}\varphi_{j,xx}\, dx \tag{35}$$

$$S_{23}(i,j) = \frac{E(x,z)}{1-\mu^2}\int_{-\frac{h}{2}}^{\frac{h}{2}} \varphi_{i,xx}\psi_{j,x}\, dx \tag{36}$$

$$S_{33}(i,j) = \frac{E(x,z)}{1-\mu^2}\int_{-\frac{h}{2}}^{\frac{h}{2}} \psi_{i,xx}\psi_{j,xx}\, dx \tag{37}$$

## 3. Numerical Results and Discussion

The numerical investigations based on HSDT are carried out to predict the static analysis of FG porous beam with various boundary conditions (BC) like simply supported (SS), clamped- clamped (CC), clamped-simply supported (CS), and clamped-free (CF).

Based on Navier's solutions, numerical results are obtained. FG porous beam is made up of Aluminum metal with modulus of elasticity ($E_m$) = 70 GPa and Poisson's ratio ($\mu_m$) = 0.3and density ($\rho_m$) = 2702 kg/m$^3$, and Alumina ceramic with young modulus ($E_c$) = 380 GPa and Poisson's ratio ($\mu_c$) = 0.3 and density ($\rho_c$) = 3960 kg/m$^3$. As per power-law distribution, FG beam properties are varying along with thickness and length directions.

### 3.1 Bending of FG Beam

For the representation of results, the following dimensionless forms are used.

Axial displacement (u)

$$\overline{u} = \frac{u100E_m h^3}{q_0 L} \tag{38}$$

Transverse displacement (w)

$$\overline{w} = \frac{w100E_m h^3}{q_0 L} \tag{39}$$

Axial stress ($\sigma_x$)

$$\overline{\sigma}_x = \frac{\sigma_x h}{q_0 L} \tag{40}$$

interpretation is due to the ductility of the beam, the exponent is increasing the beam which becomes more ductile. The results obtained at ($\varepsilon_z = 0$) are compared with other results ($\varepsilon_z = 0$) from literature such as TBT of Li et al. [8], TBT of Vo et al. [22], and TBT with FEM of Vo et al. [22]. It can also be noted that 2D higher order shear deformation theory with fifth order is in good agreement with other theories of shear deformation.

**Table 2** Assessment of dimensionless transverse deflection $\overline{\boldsymbol{w}}$ values of SS TDFG porous beam with different theories at various aspect ratios (L/h=5, L/h=20) and gradation exponents.

| Method | Theory | $\varepsilon_z$ | P=0 | P=1 | P=2 | P=5 | P=10 |
|---|---|---|---|---|---|---|---|
| L/h=5 | | | | | | | |
| Li et al.[8] | TBT | =0 | 3.1657 | 6.2559 | 8.0602 | 9.7802 | 10.8979 |
| Vo et al.[22] | TBT | =0 | 3.1654 | 6.2594 | 8.0677 | 9.8281 | 10.9381 |
| Vo et al. [FEM][22] | TBT | =0 | 3.1654 | 6.2590 | 8.0668 | 9.8271 | 10.9375 |
| present | HSDT | =0 | 3.1658 | 6.2603 | 8.0609 | 9.7806 | 10.8984 |
| L/h=20 | | | | | | | |
| Li et al.[8] | TBT | =0 | 2.8962 | 5.8049 | 7.4415 | 8.8151 | 9.6879 |
| Vo et al.[22] | TBT | =0 | 2.8962 | 5.8049 | 7.4421 | 8.8182 | 9.6905 |
| Vo et al. [FEM][22] | TBT | =0 | 2.8963 | 5.8045 | 7.4412 | 8.8173 | 9.6899 |
| present | HSDT | =0 | 2.8964 | 5.8052 | 7.4419 | 8.8158 | 9.6884 |

**Table 3** Assessment of dimensionless axial stress $\overline{\boldsymbol{\sigma}}_{\boldsymbol{x}}$ values of SS TDFG porous beam with different theories at various aspect ratios (L/h=5, L/h=20) and gradation exponents.

| Method | Theory | $\varepsilon_z$ | P=0 | P=1 | P=2 | P=5 | P=10 |
|---|---|---|---|---|---|---|---|
| L/h=5 | | | | | | | |
| Li et al.[8] | TBT | =0 | 3.8020 | 5.8837 | 6.8812 | 8.1030 | 9.7063 |
| Vo et al.[22] | TBT | =0 | 3.8020 | 5.8836 | 6.8826 | 8.1106 | 9.7122 |
| Vo et al. [FEM][22] | TBT | =0 | 3.8040 | 5.8870 | 6.8860 | 8.1150 | 9.7170 |
| present | HSDT | =0 | 3.8028 | 5.8843 | 6.8817 | 8.1035 | 9.7069 |
| L/h=20 | | | | | | | |
| Li et al.[8] | TBT | =0 | 15.0130 | 23.2054 | 27.0989 | 31.8112 | 38.1372 |
| Vo et al.[22] | TBT | =0 | 15.0129 | 23.2053 | 27.0991 | 31.8130 | 38.1385 |
| Vo et al. [FEM][22] | TBT | =0 | 15.0200 | 23.2200 | 27.1100 | 31.8300 | 38.1600 |
| present | HSDT | =0 | 15.0223 | 23.2059 | 27.0994 | 31.8117 | 38.1378 |

**Table 4** Assessment of dimensionless shear stress $\overline{\boldsymbol{\sigma}}_{\boldsymbol{xz}}$values of SS TDFG porous beam with different theories at various aspect ratios (L/h=5, L/h=20) and gradation exponents.

| Method | Theory | $\varepsilon_z$ | P=0 | P=1 | P=2 | P=5 | P=10 |
|---|---|---|---|---|---|---|---|
| L/h=5 | | | | | | | |
| Li et al.[8] | TBT | =0 | 0.7500 | 0.7500 | 0.6787 | 0.5790 | 0.6436 |
| Vo et al.[22] | TBT | =0 | 0.7332 | 0.7332 | 0.6706 | 0.5905 | 0.6467 |
| Vo et al. [FEM][22] | TBT | =0 | 0.7335 | 0.7335 | 0.6700 | 0.5907 | 0.6477 |
| Li et al.[8] | HSDT | =0 | 0.7339 | 0.7339 | 0.6698 | 0.5895 | 0.6379 |
| L/h=20 | | | | | | | |
| Li et al.[8] | TBT | =0 | 0.7500 | 0.7500 | 0.6787 | 0.5790 | 0.6436 |
| Vo et al.[22] | TBT | =0 | 0.7451 | 0.7451 | 0.6824 | 0.6023 | 0.6596 |
| Vo et al. [FEM][22] | TBT | =0 | 0.7470 | 0.7470 | 0.6777 | 0.6039 | 0.6682 |
| present | HSDT | =0 | 0.7483 | 0.7483 | 0.6781 | 0.6052 | 0.6698 |

**Table 5** Dimensionless normal stress $\overline{\sigma}_z$ values of SS TDFG beam with various aspect ratios (L/h=5, L/h=20) and gradation exponents.

| Method | Theory | $\varepsilon_z$ | P=0 | P=1 | P=2 | P=5 | P=10 |
|---|---|---|---|---|---|---|---|
| L/h=5 | | | | | | | |
| present | HSDT | =0 | 0.1378 | 0.0693 | 0.0921 | 0.0176 | -0.0168 |
| L/h=20 | | | | | | | |
| present | HSDT | =0 | 0.0344 | 0.0342 | 0.0335 | 0.0330 | 0.0328 |

It can be observed that the effect of porosity coefficient on bending behavior of FG beams subjected to uniform transverse load, transverse deflection increases as the porosity coefficient increases and this effect is more prominent with high values of porosities from 20% to 30% porosity rate and this is due to decrease in flexural rigidity of the beam with high rates of porosity [37].

**3.2.1 Two directional Simply Supported (SS) beam with Functionally Graded Porous Material:**

To analyze 2-directional SS functionally graded beam with porous under UDL at various aspect ratios and gradation exponents for finding dimensionless transverse deflections and different stresses.

**Transverse deflections:**

Table 6 presented transverse deflections at various aspect ratio (L/h=5, 20) and various gradient indexes and Table 7 presented transverse deflections at various porosity indexes.

- ❖ The values of dimensionless transverse deflections decrease with increase in the aspect ratio.
- ❖ The value of dimensionless transverse deflections increases with increase in gradation exponents in two directions.
- ❖ The transverse deflections value increases with increase in the porosity index (α) in two directions, but the value of transverse deflection is more in even porosity distribution when compare with uneven porosity distribution as seen in Figure 4.

**Table 6.** Dimensionless transverse deflection $\overline{w}$ values of SS TDFG porous beam with various aspect ratios (L/h=5, L/h=20) and gradation exponents in two directions.

| | L/h=5 | | $P_x$ | | |
|---|---|---|---|---|---|
| $P_z$ | 0 | 1 | 2 | 5 | 10 |
| 0 | 3.1658 | 4.0115 | 4.9970 | 8.2935 | 12.3255 |
| 1 | 6.2603 | 7.3828 | 8.5144 | 11.4903 | 14.3650 |
| 2 | 8.0609 | 9.08992 | 10.0844 | 12.6209 | 15.0206 |
| 5 | 9.7806 | 10.6646 | 11.5205 | 13.6706 | 15.5886 |
| 10 | 10.8984 | 11.7691 | 12.5839 | 14.4801 | 16.0113 |

| | L/h=20 | | $P_x$ | | |
|---|---|---|---|---|---|
| $P_z$ | 0 | 1 | 2 | 5 | 10 |
| 0 | 2.8964 | 3.6677 | 4.5698 | 7.6289 | 11.4158 |
| 1 | 5.8052 | 6.8284 | 7.8602 | 10.6171 | 13.3019 |
| 2 | 7.4419 | 8.3643 | 9.2636 | 11.6107 | 13.8555 |
| 5 | 8.8158 | 9.6223 | 10.4129 | 12.4901 | 14.3346 |
| 10 | 9.6884 | 10.5211 | 11.3045 | 13.1396 | 14.6662 |

**Table 7** Dimensionless transverse deflection $\overline{w}$ values of SS TDFG beam with even and uneven porosity, aspect ratio (L/h=5), and gradation exponents.

| | L/h=5 | Porosity Index(even) | | |
|---|---|---|---|---|
| $P_x$ & $P_z$ | 0 | 0.1 | 0.2 | 0.3 |
| 0 | 3.1658 | 3.4131 | 3.7029 | 4.0464 |
| 1 | 7.3828 | 7.9595 | 8.6353 | 9.4364 |
| 2 | 10.0844 | 10.8721 | 11.7952 | 12.8894 |
| 5 | 13.6706 | 14.7384 | 15.9899 | 17.4732 |
| 10 | 16.0113 | 17.2620 | 18.7277 | 20.4650 |

| | L/h=5 | Porosity Index(uneven) | | |
|---|---|---|---|---|
| $P_x$ & $P_z$ | 0 | 0.1 | 0.2 | 0.3 |
| 0 | 3.1658 | 3.2297 | 3.2967 | 3.3667 |
| 1 | 7.3828 | 7.5318 | 7.6880 | 7.8513 |
| 2 | 10.0844 | 10.2879 | 10.5013 | 10.7243 |
| 5 | 13.6706 | 13.9465 | 14.2358 | 14.5381 |
| 10 | 16.0113 | 16.3344 | 16.6733 | 17.0273 |

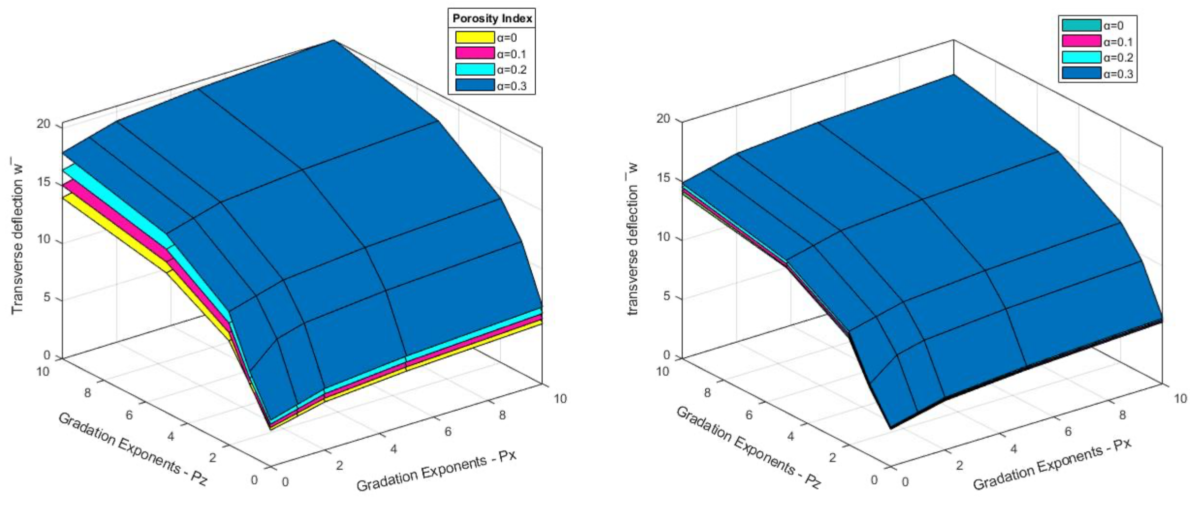


**Fig. 4** Dimensionless Transverse deflection $\overline{w}$ values of SS TDFG porous beam with even and uneven porosity, aspect ratio (L/h=5), and gradation exponents.

**Axial stress:**

Table 8 presented axial stress at various aspect ratio (L/h=5, 20) and various gradient indexes and Table 9 presented axial stress at various porosity indexes.

- ❖ Dimensionless axial stress value increases with increase in aspect ratio but decreases in both directions when increasing the gradation exponents in both directions as shown in Figure 5.
- ❖ Dimensionless axial stress value decreases with increase in porosity index in both uneven and even distribution, but dimensionless axial stress is more in even distribution when compare with uneven distribution as shown in Figure 6.

**Table 8** Dimensionless axial stress $\overline{\boldsymbol{\sigma}}_{\boldsymbol{x}}$ values of SS TDFG porous beam with various aspect ratios ( L/h=5, L/h=20) and gradation exponents in two directions.

| | **L/h=5** | | **$P_x$** | | | | | **L/h=20** | | **$P_x$** | | |
|---|---|---|---|---|---|---|---|---|---|---|---|---|
| **$P_z$** | **0** | **1** | **2** | **5** | **10** | | **$P_z$** | **0** | **1** | **2** | **5** | **10** |
| 0 | 3.8028 | 3.7953 | 3.7711 | 3.6748 | 3.6154 | | 0 | 15.0223 | 14.9971 | 14.8984 | 14.5087 | 14.2589 |
| 1 | 5.8843 | 5.6987 | 5.3479 | 4.6229 | 3.9745 | | 1 | 23.2059 | 22.1693 | 21.0825 | 18.2105 | 15.6877 |
| 2 | 6.8817 | 6.4151 | 5.9786 | 4.9472 | 4.0811 | | 2 | 27.0994 | 25.2609 | 23.5394 | 19.4678 | 16.1418 |
| 5 | 8.1035 | 7.4701 | 6.8840 | 5.4710 | 4.2457 | | 5 | 31.8117 | 29.3437 | 27.0425 | 21.5376 | 16.7825 |
| 10 | 9.7069 | 8.8409 | 8.0218 | 6.0381 | 4.3969 | | 10 | 38.1378 | 34.7751 | 31.5840 | 23.9781 | 17.3825 |

**Table 9** Dimensionless axial stress $\overline{\boldsymbol{\sigma x}}$ values of SS TDFG beam with even and uneven porosity, aspect ratio (L/h=5), and gradation exponents.

| | **L/h=5** | **porosity index(even)** | | | | | **L/h=5** | **porosity index(uneven)** | | |
|---|---|---|---|---|---|---|---|---|---|---|
| **$P_x$ & $P_z$** | **0** | **0.1** | **0.2** | **0.3** | | **$P_x$ & $P_z$** | **0** | **0.1** | **0.2** | **0.3** |
| 0 | 3.8028 | 3.8028 | 3.8028 | 3.8028 | | 0 | 3.8028 | 3.5920 | 3.3734 | 3.1461 |
| 1 | 5.6987 | 5.5321 | 5.3218 | 5.1029 | | 1 | 5.6987 | 5.3828 | 5.0552 | 4.7146 |
| 2 | 5.9786 | 5.7826 | 5.5031 | 5.3913 | | 2 | 5.9786 | 5.6471 | 5.3035 | 4.9461 |
| 5 | 5.4710 | 5.2872 | 5.0916 | 4.8375 | | 5 | 5.4710 | 5.1677 | 4.8532 | 4.5262 |
| 10 | 4.3969 | 4.2312 | 4.0837 | 3.9026 | | 10 | 4.3969 | 4.1531 | 3.9004 | 3.6376 |

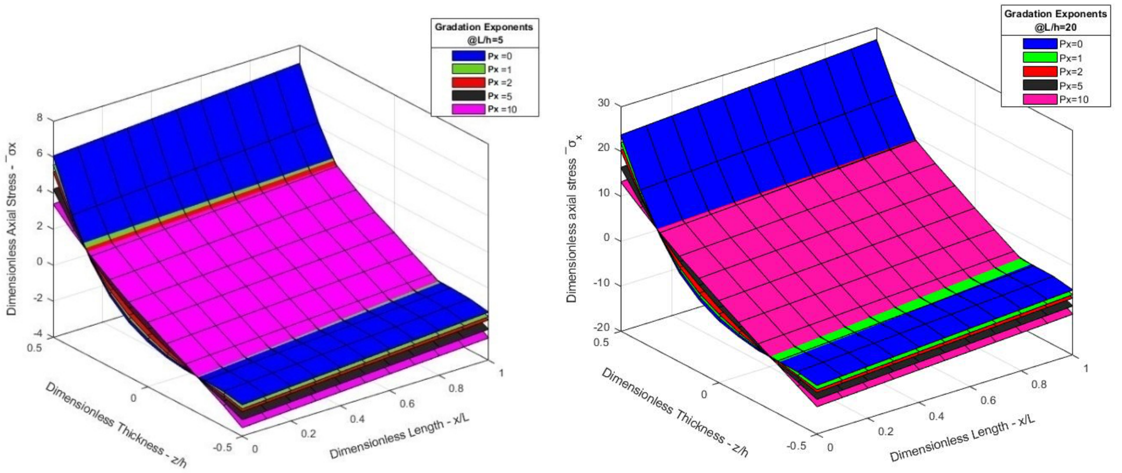


**Fig. 5** Dimensionless axial stress $\overline{\sigma}_x$ values of SS TDFG porous beam with various aspect ratios (L/h=5, L/h=20) and gradation exponents through the thickness of the beam

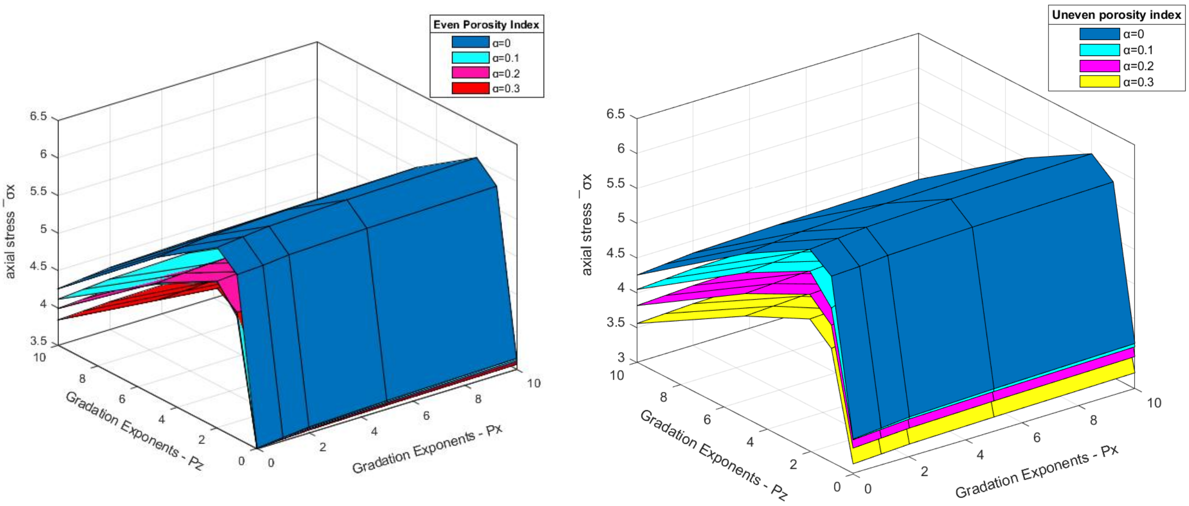


**Fig. 6** Dimensionless axial stress $\overline{\sigma_x}$ values of SS TDFG porous beam with even and uneven porosity, aspect ratio ( L/h=5), and gradation exponents.

**Shear Stress:**

Table 10 presented shear stress at various aspect ratio (L/h=5, 20) and various gradient indexes and Table 11 presented shear stress at various porosity indexes.

- ❖ The dimensionless shear stress is increasing with increase in the aspect ratio but decreases in both directions with increase in gradation exponents.
- ❖ The dimensionless shear stress value is maximum at $P_z$=0 and $P_x$=5 as shown in Figure 7.
- ❖ Dimensionless shear stress value increases with increase in the porosity index in even distribution but decreases in the uneven porosity distribution. When compare shear stress value is less in uneven porosity distribution than even porosity distribution as shown in Figure 8.

**Table 10** Dimensionless shear stress $\overline{\sigma}_{xz}$ values of SS TDFG porous beam with various aspect ratios ( L/h=5, L/h=20) and gradation exponents in two directions.

| | L/h=5 | | $P_x$ | | |
|---|---|---|---|---|---|
| $P_z$ | 0 | 1 | 2 | 5 | 10 |
| 0 | 0.7339 | 0.8025 | 0.8593 | 0.9397 | 0.9313 |
| 1 | 0.7339 | 0.7893 | 0.8305 | 0.8788 | 0.8684 |
| 2 | 0.6698 | 0.7102 | 0.7378 | 0.7674 | 0.7614 |
| 5 | 0.5895 | 0.6058 | 0.6156 | 0.6261 | 0.6258 |
| 10 | 0.6379 | 0.6440 | 0.6477 | 0.6525 | 0.6540 |

| | L/h=20 | | $P_x$ | | |
|---|---|---|---|---|---|
| $P_z$ | 0 | 1 | 2 | 5 | 10 |
| 0 | 0.7483 | 0.8188 | 0.8786 | 0.9655 | 0.9541 |
| 1 | 0.7483 | 0.8048 | 0.8473 | 0.8962 | 0.8838 |
| 2 | 0.6781 | 0.7191 | 0.7477 | 0.7783 | 0.7731 |
| 5 | 0.6052 | 0.6238 | 0.6380 | 0.6401 | 0.6430 |
| 10 | 0.6698 | 0.6779 | 0.6843 | 0.6832 | 0.6886 |

**Table 11** Dimensionless shear stress $\overline{\sigma xz}$ values of SS TDFG beam with even and uneven porosity, aspect ratio (L/h=5), and gradation exponents.

| $P_x$ & $P_z$ | L/h=5 | porosity index(even) | | |
|---|---|---|---|---|
| | 0 | 0.1 | 0.2 | 0.3 |
| 0 | 0.7339 | 0.7339 | 0.7339 | 0.7339 |
| 1 | 0.7360 | 0.7364 | 0.7370 | 0.7382 |
| 2 | 0.7443 | 0.7459 | 0.7484 | 0.7524 |
| 5 | 0.7625 | 0.7644 | 0.7660 | 0.7671 |
| 10 | 0.7453 | 0.7432 | 0.7501 | 0.7548 |

| $P_x$ & $P_z$ | L/h=5 | porosity index(uneven) | | |
|---|---|---|---|---|
| | 0 | 0.1 | 0.2 | 0.3 |
| 0 | 0.7339 | 0.6964 | 0.6505 | 0.5923 |
| 1 | 0.7360 | 0.7051 | 0.6684 | 0.6240 |
| 2 | 0.7443 | 0.7159 | 0.6828 | 0.6437 |
| 5 | 0.7505 | 0.725 | 0.6961 | 0.6636 |
| 10 | 0.7453 | 0.7202 | 0.6918 | 0.6595 |

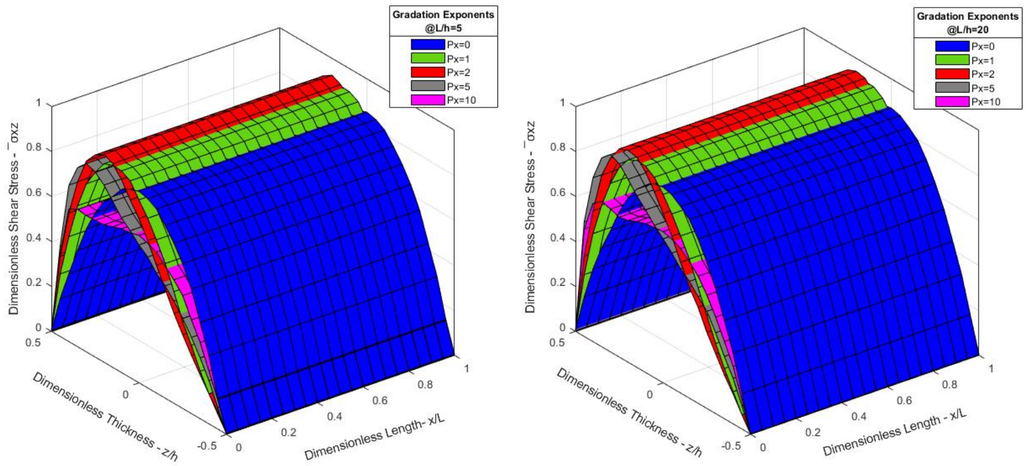


**Fig. 7** Dimensionless shear stress $\overline{\sigma}_{xz}$ values of SS TDFG porous beam with various aspect ratios (L/h=5, L/h=20) and gradation exponents through the thickness of the beam.

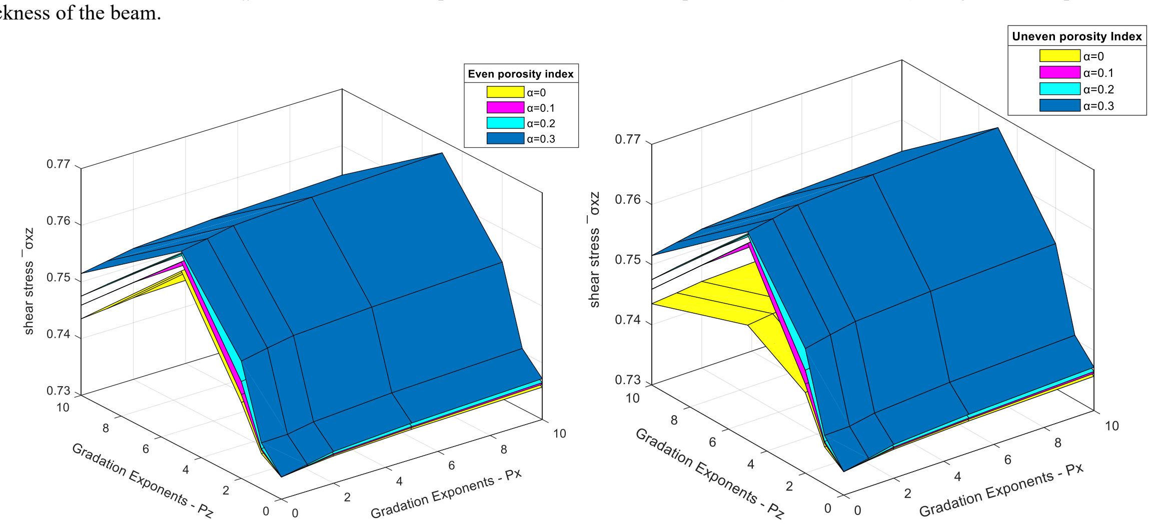


**Fig. 8** Dimensionless shear stress $\overline{\sigma_{xz}}$ values of SS TDFG porous beam with even and uneven porosity, aspect ratio ( L/h=5), and gradation exponents

**Normal stress:**
Table 12 presented normal stress at various aspect ratio (L/h=5, 20) and various gradient indexes and Table 13 presented normal stress at various porosity indexes.

- ❖ At aspect ratio 20, the dimensionless normal stress value is almost vanished except at gradation exponent at zero in Z- direction as shown in Figure 9.
- ❖ Normal stress value decreases with increase in gradation exponent and also decreases with increase in porosity in both uneven and even distribution but value of normal stress is more in even distribution compared with uneven distribution as shown in Figure 10.

**Table 12** Dimensionless Normal stress $\overline{\sigma}_z$ values of SS TDFG porous beam with various aspect ratios (L/h=5, L/h=20) and gradation exponents in two directions.

| $P_z$ | L/h=5 | | $P_x$ | | |
|---|---|---|---|---|---|
| | 0 | 1 | 2 | 5 | 10 |
| 0 | 0.1378 | 0.1375 | 0.1371 | 0.1356 | 0.1353 |
| 1 | 0.0693 | 0.0571 | 0.0514 | 0.0656 | 0.1120 |
| 2 | 0.0921 | 0.0580 | 0.0420 | 0.0574 | 0.1105 |
| 5 | 0.0176 | 0.0104 | 0.0198 | 0.0746 | 0.1212 |
| 10 | -0.0168 | 0.0146 | 0.0464 | 0.1097 | 0.1303 |

| $P_z$ | L/h=20 | | $P_x$ | | |
|---|---|---|---|---|---|
| | 0 | 1 | 2 | 5 | 10 |
| 0 | 0.0342 | 0.0342 | 0.0340 | 0.0336 | 0.0335 |
| 1 | -0.5885 | -0.6020 | -0.5869 | -0.4232 | -0.1164 |
| 2 | -0.6253 | -0.7093 | -0.7164 | -0.5033 | -0.1135 |
| 5 | -1.1689 | -1.0996 | -0.9642 | -0.5059 | -0.0841 |
| 10 | -1.5571 | -1.2667 | -0.9850 | -0.3455 | -0.0492 |

**Table 13** Dimensionless Normal stress $\overline{\sigma z}$ values of SS TDFG beam with even and uneven porosity, aspect ratio (L/h=5), and gradation exponents.

| $P_x$ & $P_z$ | L/h=5 | porosity index(even) | | |
|---|---|---|---|---|
| | 0 | 0.1 | 0.2 | 0.3 |
| 0 | 0.1378 | 0.1378 | 0.1378 | 0.1378 |
| 1 | 0.0571 | 0.0556 | 0.0502 | 0.0469 |
| 2 | 0.0420 | 0.0396 | 0.0377 | 0.0339 |
| 5 | 0.0746 | 0.0730 | 0.0704 | 0.0650 |
| 10 | 0.1303 | 0.1275 | 0.1229 | 0.1135 |

| $P_x$ & $P_z$ | L/h=5 | porosity index(uneven) | | |
|---|---|---|---|---|
| | 0 | 0.1 | 0.2 | 0.3 |
| 0 | 0.1378 | 0.1281 | 0.1185 | 0.1087 |
| 1 | 0.0571 | 0.0530 | 0.0491 | 0.0450 |
| 2 | 0.0420 | 0.0530 | 0.0361 | 0.0331 |
| 5 | 0.0746 | 0.0693 | 0.0641 | 0.0588 |
| 10 | 0.1303 | 0.1211 | 0.1120 | 0.1027 |

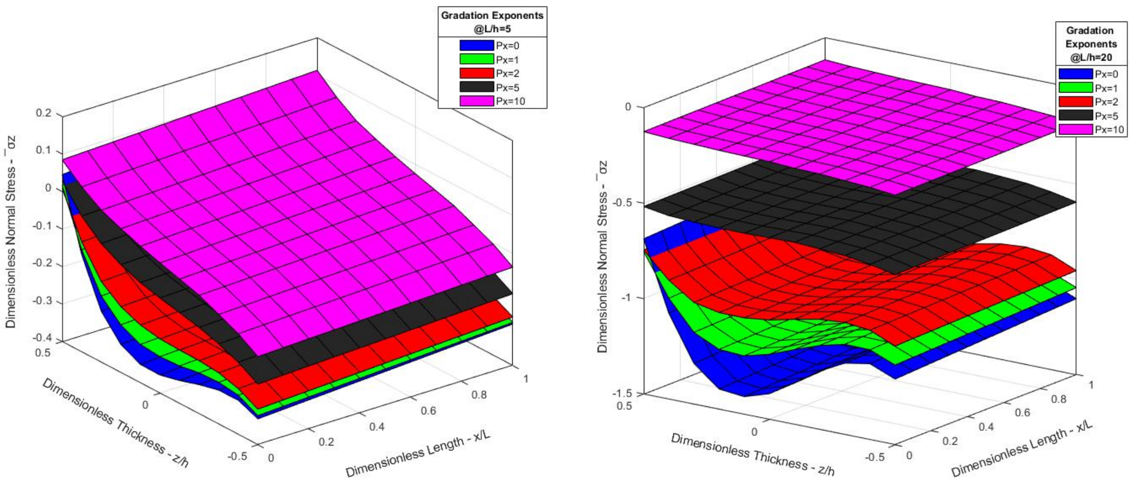


**Fig. 9** Dimensionless normal stress $\overline{\sigma}_z$ values of SS TDFG porous beam with various aspect ratios (L/h=5, L/h=20) and gradation exponents through the thickness of the beam.

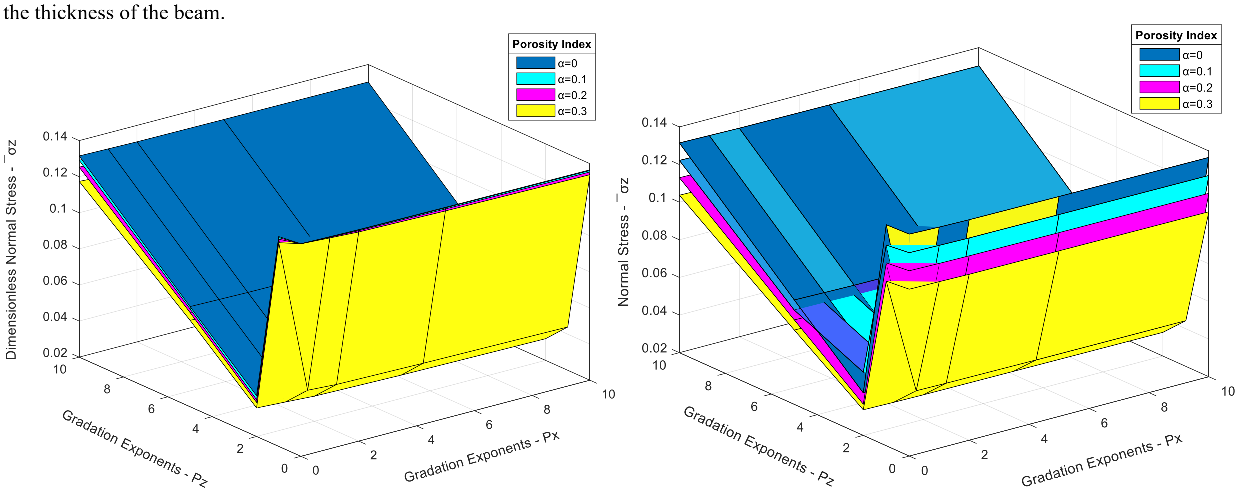


**Fig. 10** Dimensionless Normal stress $\overline{\sigma}_z$ values of SS TDFG porous beam with even and uneven porosity, aspect ratio ( L/h=5), and gradation exponents.

### 3.2.2 Two Directional Clamped-Simply Supported (CS) Beam With Functionally Graded Porous Material

**Transverse deflections:**

To analyze clamped – simply supported two-directional functionally graded porous beam to find dimensionless transverse deflection, axial stress, normal stress, and shear stress at different aspect ratios and gradation exponents.

Table 14 presented transverse deflection at various aspect ratio (L/h=5, 20) and various gradient indexes and Table 15 presented transverse deflections at various porosity indexes.

- ❖ Transverse deflection value increases with increase aspect ratio in x and z directions but the value of transverse deflection is high at a lower aspect ratio compared to higher aspect ratio.
- ❖ Concerning porosity index, the transverse deflection values are increasing with increase in porosity index in even and uneven distribution but the transverse deflection value is more in even distribution as compared to uneven distribution as shown in Figure 11.

**Table 14** Dimensionless transverse deflections $\overline{w}$ values of CS TDFG porous beam with various aspect ratios (L/h=5, L/h=20) and gradation exponents in two directions

| | L/h=5 | | $P_x$ | | | | | L/h=20 | | $P_x$ | | |
|---|---|---|---|---|---|---|---|---|---|---|---|---|
| $P_z$ | 0 | 1 | 2 | 5 | 10 | | $P_z$ | 0 | 1 | 2 | 5 | 10 |
| 0 | 1.4502 | 1.7988 | 2.1849 | 3.3263 | 4.4763 | | 0 | 1.2577 | 1.5303 | 1.8342 | 2.7519 | 3.6937 |
| 1 | 2.7956 | 3.2551 | 3.702 | 4.7672 | 5.6626 | | 1 | 2.2580 | 2.6619 | 3.0411 | 3.8841 | 4.7255 |
| 2 | 3.6061 | 4.0384 | 4.4392 | 5.3688 | 6.1148 | | 2 | 2.8631 | 3.2666 | 3.6276 | 4.3325 | 4.9963 |
| 5 | 4.5451 | 4.9033 | 5.2365 | 5.9822 | 6.5463 | | 5 | 3.2456 | 3.6316 | 3.8931 | 4.594 | 5.2985 |
| 10 | 5.1535 | 5.4771 | 5.7674 | 6.3862 | 6.8246 | | 10 | 3.8219 | 4.1559 | 4.3407 | 4.9696 | 5.6270 |

**Table 15** Dimensionless transverse deflections $\overline{w}$ values of CS TDFG beam with even and uneven porosity, aspect ratio (L/h=5), and gradation exponents

| $P_x$ & $P_z$ | L/h=5 | porosity index(even) | | | | $P_x$ & $P_z$ | L/h=5 | porosity index(uneven) | | |
|---|---|---|---|---|---|---|---|---|---|---|
| | 0 | 0.1 | 0.2 | 0.3 | | | 0 | 0.1 | 0.2 | 0.3 |
| 0 | 1.4502 | 1.5635 | 1.6963 | 1.8537 | | 0 | 1.4502 | 1.5224 | 1.6027 | 1.6924 |
| 1 | 3.2551 | 3.5098 | 3.8080 | 4.1613 | | 1 | 3.2551 | 3.4176 | 3.5978 | 3.7992 |
| 2 | 4.4392 | 4.7865 | 5.1932 | 5.675 | | 2 | 4.4392 | 4.6608 | 4.9066 | 5.1813 |
| 5 | 5.9822 | 6.4502 | 6.9983 | 7.6476 | | 5 | 5.9822 | 6.2808 | 6.6121 | 6.9822 |
| 10 | 6.8246 | 7.3586 | 7.9838 | 8.7245 | | 10 | 6.8246 | 7.1653 | 7.5433 | 7.9654 |

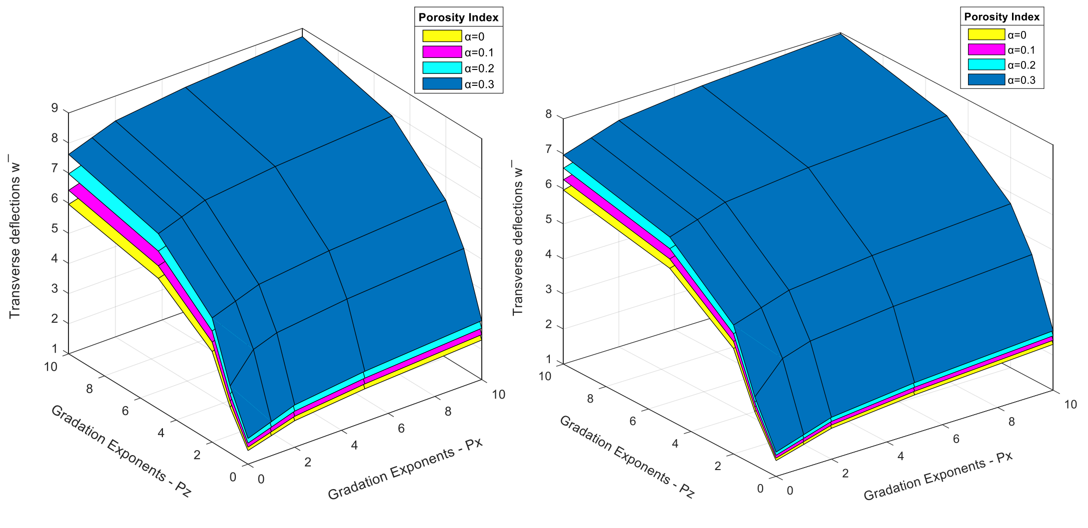


**Fig. 11** Dimensionless Transverse deflections $\overline{w}$ values of CS TDFG porous beam with even and uneven porosity, aspect ratio (L/h=5), and gradation exponents.

**Axial stress:**

Observed from Figure 12,

- ❖ Axial stress value is maximum at aspect ratio of 20.
- ❖ Axial stress value is maximum at the top of beam.

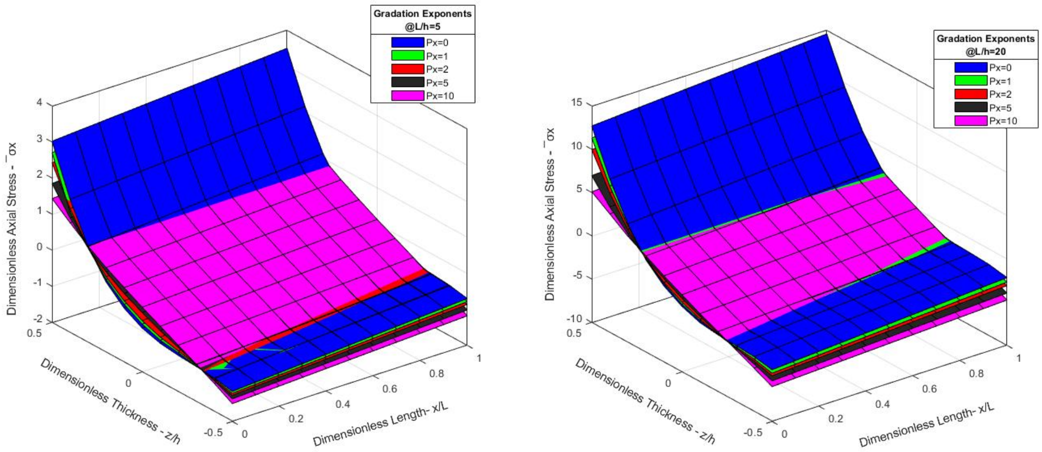


**Fig. 12** Dimensionless axial stress $\overline{\sigma}_x$ values of CS TDFG porous beam with various aspect ratios (L/h=5, L/h=20) and gradation exponents through the thickness of the beam.

**Shear stress:**
Observed from Figure 13,

- ❖ The value of shear stress is increasing with increase in aspect ratio.
- ❖ Shear stress of beam is maximum at the middle of beam.

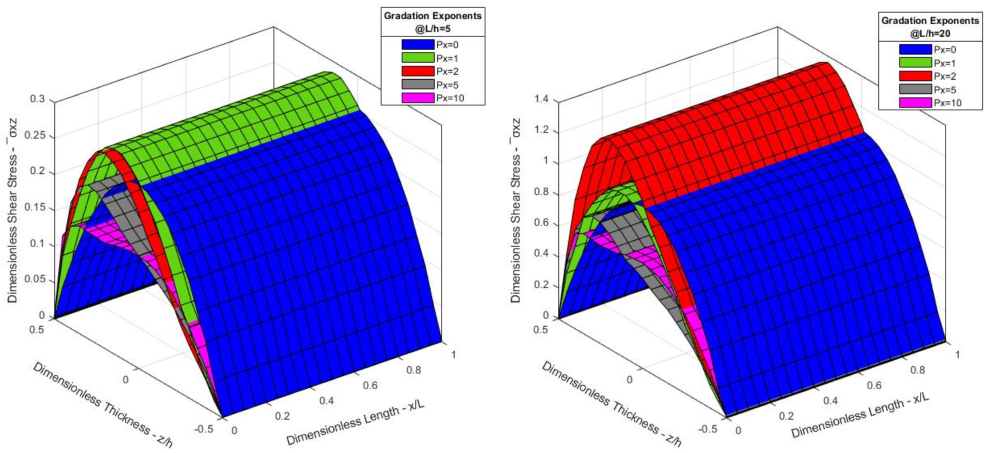


**Fig. 13** Dimensionless Shear stress $\overline{\sigma}_{xz}$ values of CS TDFG porous beam with various aspect ratios (L/h=5, L/h=20) and gradation exponents along with the thickness of the beam.

**Normal Stress:**
Observed from Figure 14,

- ❖ The Normal stress value decreases with increase in the aspect ratio.
- ❖ The maximum normal stress value is at the top of the beam.

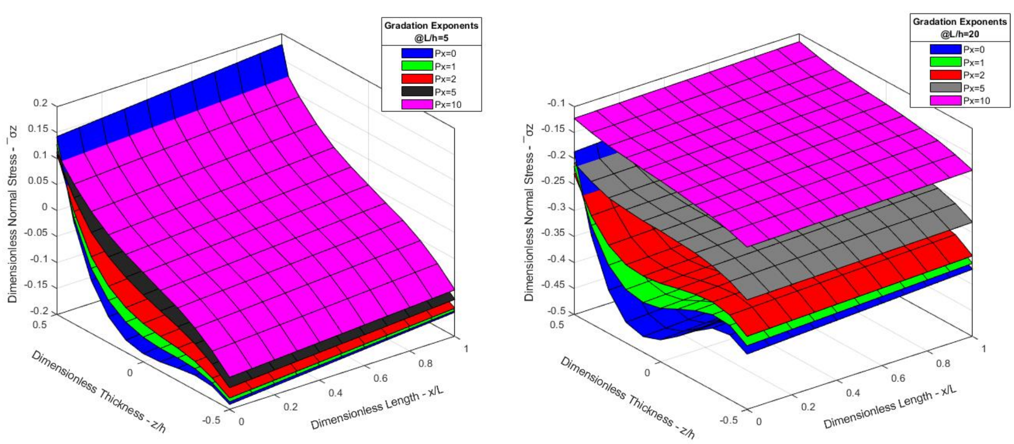


**Fig. 14** Dimensionless Normal stress $\overline{\sigma}_z$ values of CS TDFG porous beam with different aspect ratios (L/h=5, L/h=20) and gradation exponents along with the thickness of the beam.

### 3.2.3 Two Directional Clamped - Clamped (CC) Beam with Functionally Graded Porous Material

**Transverse deflections:**
Two-directional Clamped-Clamped functionally graded porous beam is analyzed for finding transverse deflection, axial stress, normal stress, and shear stress with different aspect ratios and gradation exponents in 2-directions.

Table 16 presented transverse deflection at various aspect ratios (L/h=5, 20) and various gradation exponents and Table 17 presented transverse deflection at various porosity indexes.

- ❖ Transverse deflection increases with increase gradation exponent in two directions and transverse deflection decreases with increase in aspect ratio.
- ❖ Transverse deflection increases with increase in porosity index in both even and uneven distribution but the maximum value is found at even distribution as shown in Figure 15.

**Table 16** Dimensionless Transverse deflections $\overline{w}$ values of CC TDFG porous beam with various aspect ratios (L/h=5, L/h=20) and gradation exponents in two directions

| | L/h=5 | $P_x$ | | | | | | L/h=20 | $P_x$ | | | |
|---|---|---|---|---|---|---|---|---|---|---|---|---|
| $P_z$ | 0 | 1 | 2 | 5 | 10 | | $P_z$ | 0 | 1 | 2 | 5 | 10 |
| 0 | 0.8349 | 1.0662 | 1.3189 | 2.0192 | 2.6770 | | 0 | 0.5899 | 0.7536 | 0.9320 | 1.4191 | 1.8581 |
| 1 | 1.5870 | 1.8837 | 2.1659 | 2.8111 | 3.3069 | | 1 | 1.1632 | 1.3759 | 1.5743 | 2.0117 | 2.3397 |
| 2 | 2.0810 | 2.3586 | 2.6102 | 3.1765 | 3.5774 | | 2 | 1.4910 | 1.6771 | 1.8515 | 2.2313 | 2.5071 |
| 5 | 2.7181 | 2.9394 | 3.1599 | 3.5876 | 3.8635 | | 5 | 1.7768 | 1.9481 | 2.1069 | 2.4413 | 2.6539 |
| 10 | 3.1105 | 3.3218 | 3.4990 | 3.8292 | 4.0289 | | 10 | 1.9699 | 1.9742 | 2.1483 | 2.3002 | 2.7623 |

**Table 17** Dimensionless Transverse deflections $\overline{w}$ values of CC TDFG beam with even and uneven porosity, aspect ratio (L/h=5), and gradation exponents.

| | Porosity Index(even) | | | | | | Porosity Index(uneven) | | | |
|---|---|---|---|---|---|---|---|---|---|---|
| $P_x$ & $P_z$ | 0 | 0.1 | 0.2 | 0.3 | | $P_x$ & $P_z$ | 0 | 0.1 | 0.2 | 0.3 |
| 0 | 0.8349 | 0.9002 | 0.9767 | 1.0673 | | 0 | 0.8349 | 0.8532 | 0.8727 | 0.8934 |
| 1 | 1.8837 | 2.0310 | 2.2036 | 2.4080 | | 1 | 1.8837 | 1.9250 | 1.9690 | 2.0157 |
| 2 | 2.6102 | 2.8144 | 3.0535 | 3.3368 | | 2 | 2.6102 | 2.6674 | 2.7284 | 2.7931 |
| 5 | 3.5876 | 3.8682 | 4.1969 | 4.5862 | | 5 | 3.5876 | 3.6662 | 3.7500 | 3.8390 |
| 10 | 4.0289 | 4.3440 | 4.7132 | 5.1504 | | 10 | 4.0289 | 4.1172 | 4.2113 | 4.3112 |

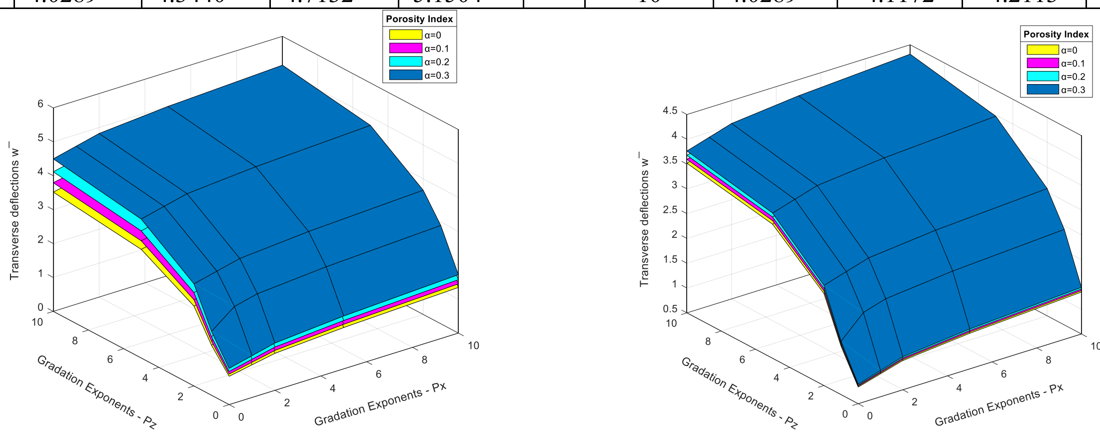


**Fig. 15** Dimensionless Transverse deflections $\overline{w}$ values of CC TDFG porous beam with even and uneven porosity, aspect ratio (L/h=5), and gradation exponents.

**Axial stress:**
Observed from Figure 16a,

- ❖ Axial stress of beam is maximum at top and maximum axial stress is at gradation exponent is zero in Z- direction.

**Shear stress:**
Observed from Figure 16b,

- ❖ The value of shear stress is maximum at the middle of the beam and the shear stress value is maximum at gradation exponent is one in Z-direction.

**Normal stress:**
Observed from Figure 16c,

- ❖ The normal stress value is maximum at top of beam and value of normal stress is maximum at gradation exponent is one in Z-direction.

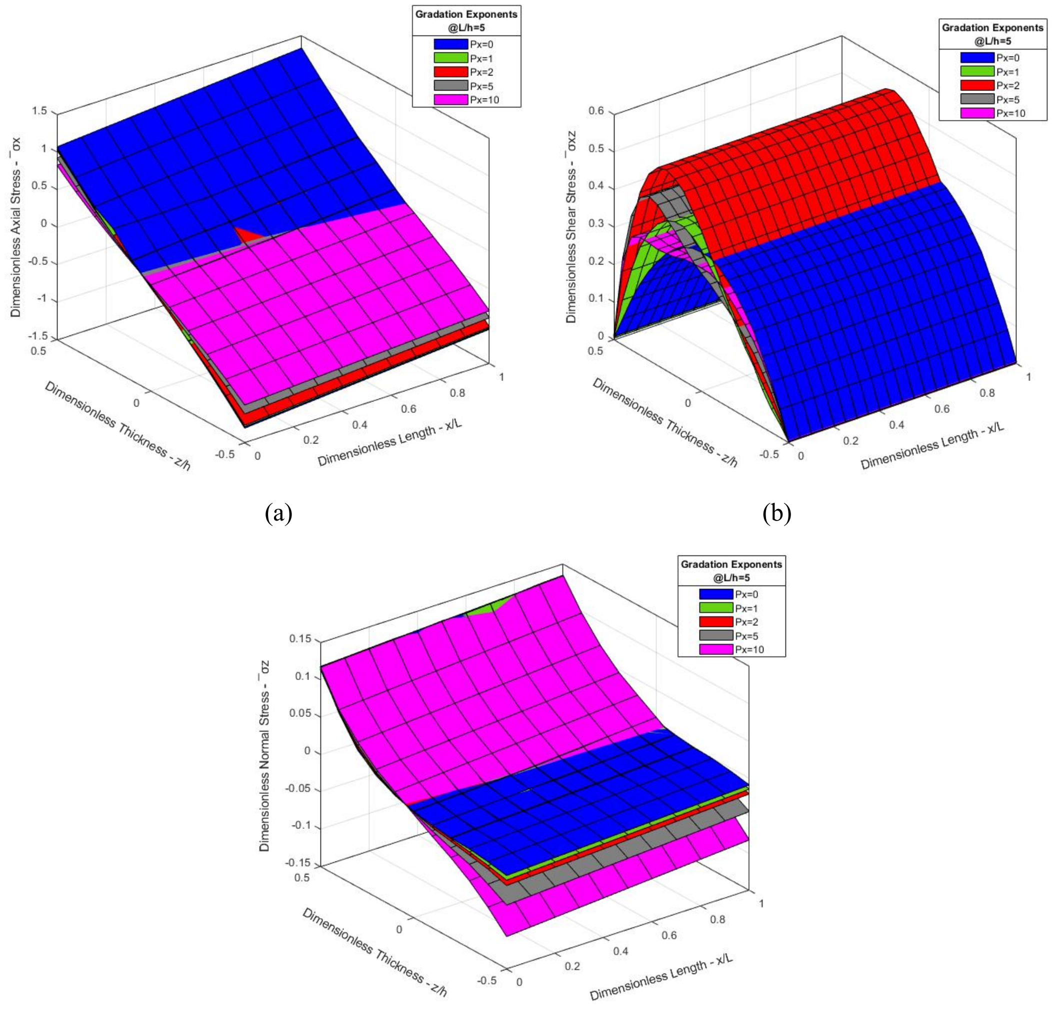


(a) (b)

(c)

**Fig. 16** Dimensionless axial stress $\overline{\sigma}_x$ $(a)$, shear stress $\overline{\sigma}_{xz}$ $(b)$, and normal stress $\overline{\sigma}_z$ (c) values of CC TDFG porous beam with a different aspect ratio ( L/h=5) and gradation exponents through the thickness of the beam.

### 3.2.4 Two directional Clamped - Free (CF) beam with functionally graded porous material

Transverse deflections:

2-directional Clamped–Free FG porous beams are tested with UDL to calculating numerical values of transverse deflection, axial stress, shear stress, and normal stress at different aspect ratios and gradation exponents.

Table 18 presented transverse deflection at various aspect ratios (L/h=5, 20) and at various gradation exponents and Table 19 presented transverse deflection at various porosity indexes.

- ❖ Dimensionless transverse deflection decreases with increase in aspect ratio but dimensionless transverse deflection increases along with gradation exponents. The values of transverse deflection cannot be accepted when aspect ratio is more than five and gradation exponents are more than two in x-direction.
- ❖ Transverse deflection value increases with increase in porosity index and gradation exponents as shown in Figure 17.
- ❖ Transverse deflection value is more in even porosity when compared to uneven porosity distribution.

**Table 18** Dimensionless Transverse deflections $\overline{\boldsymbol{w}}$ values of CF TDFG porous beam with various aspect ratios (L/h=5, L/h=20) and gradation exponents in two directions

| | **L/h=5** | | **$P_x$** | | | | | **L/h=20** | | **$P_x$** | | |
|---|---|---|---|---|---|---|---|---|---|---|---|---|
| **$P_z$** | **0** | **1** | **2** | **5** | **10** | | **$P_z$** | **0** | **1** | **2** | **5** | **10** |
| 0 | 27.1345 | 29.9112 | 32.9635 | 43.9171 | 62.5264 | | 0 | 8.5281 | 9.4008 | 10.3617 | 13.7405 | 19.6515 |
| 1 | 54.8617 | 58.2429 | 61.8219 | 72.9454 | 90.1593 | | 1 | 17.2426 | 18.3052 | 19.4301 | 22.9262 | 28.3363 |
| 2 | 74.1327 | 77.8481 | 81.4729 | 92.0133 | 107.5858 | | 2 | 23.2993 | 24.4670 | 25.6063 | 28.9190 | 33.8133 |
| 5 | 87.1959 | 90.4441 | 93.6054 | 103.4466 | 115.0084 | | 5 | 27.4098 | 28.4309 | 29.4246 | 32.8181 | 36.1525 |
| 10 | 94.4979 | 97.7456 | 100.8107 | 109.8893 | 119.2928 | | 10 | 29.7051 | 30.7260 | 31.6895 | 34.5433 | 37.4992 |

**Table 19** Dimensionless Transverse deflections $\overline{\boldsymbol{w}}$ values of CF TDFG beam with uneven and even porosity, aspect ratio (L/h=5), and gradation exponents.

| $P_x$ & $P_z$ | Porosity Index (even) | | | | $P_x$ & $P_z$ | Porosity Index (uneven) | | | |
|---|---|---|---|---|---|---|---|---|---|
| | 0 | 0.1 | 0.2 | 0.3 | | 0 | 0.1 | 0.2 | 0.3 |
| 0 | 27.1345 | 29.2581 | 31.7423 | 34.6874 | 0 | 27.1345 | 27.7741 | 28.4562 | 29.1858 |
| 1 | 58.2429 | 62.8010 | 68.1332 | 74.4548 | 1 | 58.2429 | 59.6156 | 61.0798 | 62.6459 |
| 2 | 81.4729 | 87.8490 | 95.3094 | 104.1509 | 2 | 81.4729 | 83.3932 | 85.4412 | 87.6321 |
| 5 | 103.4466 | 111.5424 | 121.0130 | 132.2410 | 5 | 103.4466 | 105.8488 | 108.4853 | 111.2670 |
| 10 | 119.2928 | 128.6288 | 139.5501 | 152.4980 | 10 | 119.2928 | 122.1045 | 125.1034 | 128.3112 |

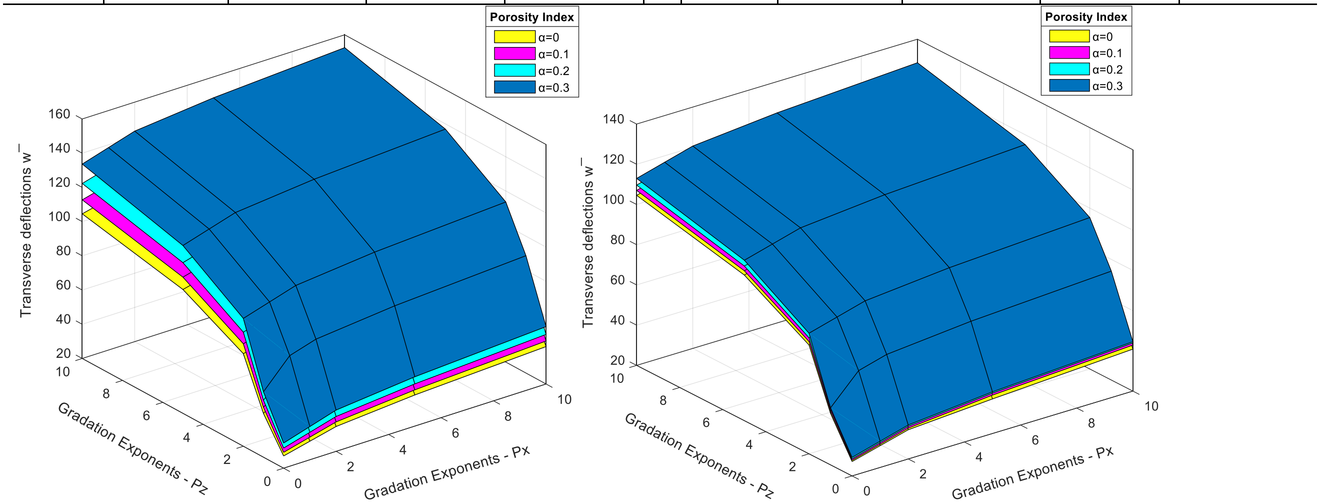


**Fig. 17** Dimensionless Transverse deflections $\overline{w}$ values of CF TDFG porous beam with even and uneven porosity, aspect ratio (L/h=5), and gradation exponents.

**Axial stress:**

Observed from Figure 18a,

- ❖ Axial stress decreases along with its thickness from bottom of the beam to the top of beam i.e. axial stress maximum at bottom of the beam and axial stress is maximum at gradation exponent of 10.

**Shear stress:**

Observed from Figure 18b,

- ❖ Shear stress is Zero at top and bottom of beam and maximum at gradation exponent 2.

**Normal stress:**

Observed from Figure 18c,

- ❖ Maximum normal stress is at top of beam and normal stress maximum at gradation exponent is zero.

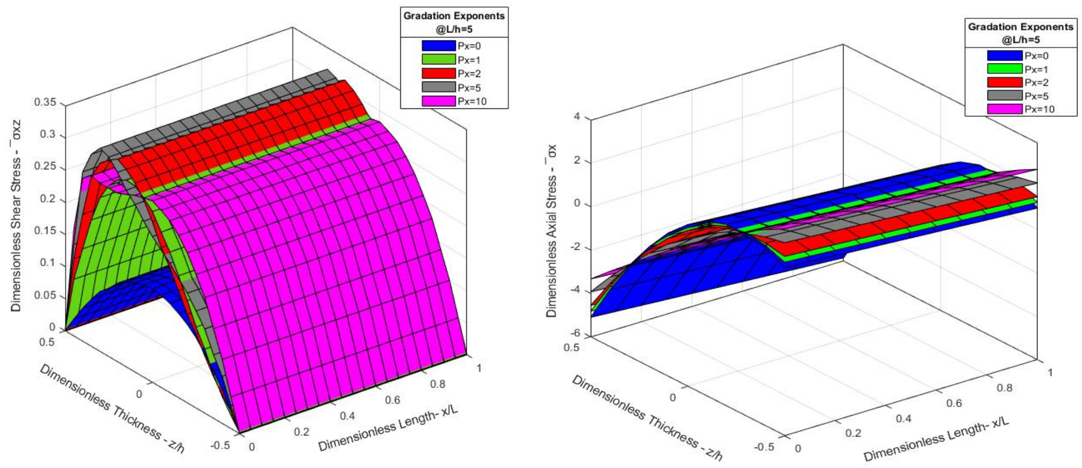


(a) (b)

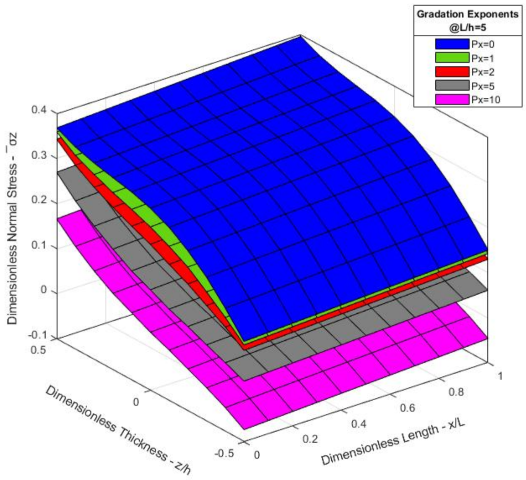


(c)

**Fig. 18** Dimensionless axial stress $\overline{\sigma}_x$ $(a)$, shear stress $\overline{\sigma}_{xz}$ $(b)$, and normal stress $\overline{\sigma}_z$ (c)values of CF TDFG porous beam with a different aspect ratio ( L/h=5) and gradation exponents through the thickness of the beam.

## 4. Conclusion

Two directional FG porous beams are analyzed for static behavior and subjected to various boundary conditions (SS, CS, CC, and CF) with UDL. Considered these boundary conditions with different aspect ratios and gradation exponents in x and z directions.

Developed 5$^{th}$ order shear deformation theory, to determining shear, axial, normal stresses and transverse deflections with thickness stretching effect on even and uneven porosity distribution.

Help of power-law distribution to determine effective properties of FG porous beams in two directions. To highlighted the effect of boundary conditions, distribution of porosity, aspect ratios, and gradation exponents on transverse deflections, axial, normal, and shear stresses. Through several numerical illustrations leading to trace that the porosity parameter is a crucial parameter that must be considered in design of modern structures and the percentage of porosity in structure can be effected considerably in its performance and response.



## References


1. Y. Huang and Z. Y. Ouyang, Arch Appl Mech, 90 (2020)
2. L. Hadji and F. Bernard, Adv. Mater. Res, 9 (2020)
3. N. Hebbar, I.Hebbar, D. Ouinas and Md. Bourada, Frattura ed Integrità Strutturale, 52 (2020).
4. A. Razouki, L. Boutahar and K. E. Bikri, Int J Adv Res Sci Eng Technol., 11 (2020).
5. P. V. Avhada and A. S. Sayyad, Mater. Today:. Proc, 21 (2020).
6. S. Coskun, J. Kim and H. Toutanji, J. Compos. Sci. 3 (2019).
7. A. A. Daikh and A. M. Zenkour, Mater. Res. Express, 6 (2019).
8. X. F. Li, B. L. Wang and J. C. Han, Arch Appl Mech, 80 (2010).
9. R.A. Sayyad, V.R. Rathi and P.K. Kolase, Int. Res J Eng Technol., 06 (2019).
10. M. Babaei, K. Asemi and P. Safarpour, Iran. J Mech Eng. 20 (2019).
11. H. N. Nguyen, T. T. Hong, P. V. Vinh, N. D. Quang and D. V. Thom, Materials 12 (2019).
12. S. Merdaci and H. Belghoul, C.R. Mec. 347 (2019).
13. A. M. Zenkour and A. F. Radwan, Compos. Struct. 213 (2019).
14. A. S. Sayyad and Y. M. Ghugal, Mech adv compos. Struct. 5 (2018).
15. J. Kim, K. Kamil Zur and J.N. Reddy, Compos. Struct. 5 (2018).
16. B. Sidda Reddy, K. Vijaya Kumar Reddy and B. Chinna Ankanna J Comp Applied Mechanics, 51 (2020).
17. M. Slimane, Alger. J Res. Technol. 2 (2018).
18. M. Jain, M.Y. Yasin, Proc. Int. Conf. Mater. Sci. Eng. 404 (2018).
19. M. Slimane, Adv. Eng. For, 30 (2018).
20. Z. F. Zohra, H. H. A. Lemya, Y. Abderahman, M. Mustapha, T. Abdelouahed and O. Djamel, Int. Info Eng Technol. Assoc, 4 (2017)
21. A. S. Sayyad and Y. M. Ghugal, Int J Appl Mechanics, 9 (2017).
22. T.P. Vo, H. T. Thai, T. K. Nguyen, F. Inam and J. Lee, Composites, Part B, 68 (2015).
23. S. M. Ghumare, A. S. Sayyad Latin American J Sol. Struct. 14 (2017).
24. S. M. Aldousari, Appl. Phys. A, 123 (2017).
25. M. T. Tran, H. Q. Tran and V.L. Nguyen, Struct. Eng. Mech. 62 (2017).
26. D. Chen, J. Yang, S. Kitipornchai, Compos. Struct. 133 (2015).
27. A. Apuzzo, R. Barretta and R. Luciano, Composites, Part B, 68 (2015).
28. R. Kolahchi, A. M. M. Bidgoli and M. M. Heydari, Struct Eng Mech, 55 (2015).
29. T. P. Vo, H. T. Thai, T. K. Nguyen, and F. Inam, Meccanica. 49 (2014a).
30. B. Sidda Reddy, J. Suresh Kumar, C. Eswara Reddy and K. Vijaya Kumar Reddy, Int. J Appl Sci and Eng 12 (2014).
31. A. karamanli, Compos. Struct. 189(2018).
32. M. Talha and B.N. Singh, Appl. Math. Modell. 34 (2010).
33. H. T. Thai and T. P. Vo, Int. J.Mech. Sci, 62 (2012).
34. T. K. Nguyen, T. P. Vo and H. T. Thai, Composites, part B, 55 (2013).
35. H. Bellifa, K.H. Benrahou, L. Hadji, M.S.A. Houari, and A. Tounsi, J Braz. Soc. Mech. Sci. Eng. 38 (2015)
36. J. Kim, K. K. Zur and J.N. Reddy, Compos. Struct. 209 (2018).
37. S. Zghal, D. Ataoui and F. Dammak, Mechanics Based Design of Structures and Machines. 50 (2020).